Parametric Representation of the Primary Hurricane Vortex. Part I: Observations and Evaluation of the Holland (1980) Model

H. E. WILLOUGHBY

International Hurricane Research Center, Florida International University, Miami, Florida

M. E. RAHN

Hurricane Research Division/AOML/NOAA, Miami, Florida

(Manuscript received 16 January 2004, in final form 1 June 2004)

ABSTRACT

Although numerical models are essential to hurricane forecasting, many other applications require only statistical depiction of the wind distribution. In Holland's 1980 parametric profile, radius of maximum wind, maximum wind, and a measure of the profile width describe the radial variation of the axisymmetric wind. Variants of the Holland profile are used to predict insurance underwriting risk, ocean response, and storm-surge inundation. Since these calculations guide high-stakes financial and emergency managment decisions, it is logical to test them against observations.

The Hurricane Research Division's flight-level database archives observations were obtained by NOAA and U.S. Air Force Reserve aircraft. The data considered here are winds and geopotential heights observed during 606 lower- and midtropospheric flights into Atlantic and eastern Pacific tropical cyclones during 1977–2000. The 493 profiles that meet quality control criteria are seasonally geographically representative.

Least squares fits of the Holland model to these data provide evaluation of the parameters' distributions and critical examination of the profile's realism. Individual fitted profiles differ from the observations in a consistent pattern. The areas of strong winds in the eyewall and of nearly calm winds at the vortex center are too wide. Beyond 2 or 3 times the eye radius, the wind decreases too rapidly with distance from the center. Although the average bias in fitted profiles is <1 m s^{-1}, the root-mean-square error is 4.2 m s^{-1} (5.2 m s^{-1} for independent data). Maximum winds estimated from the fitted Holland-profile height–wind relation average 2.5 m s^{-1} too strong with an rms error of 6.5 m s^{-1}. The pattern of too strong wind spread over too much real estate exaggerates the occurrence of winds stronger than 50 m s^{-1} by $\sim$50%.

1. Introduction

In a ''parametric'' model, the radial variation of hurricane wind depends upon the values of a few parameters, such as the maximum wind or the radius at which the maximum wind occurs. Parametric models from the basis of many statistical assessments of hazards to life and property posed by wind itself, storm surge, and ocean waves. The problem has great economic significance to the United States because landfalling hurricanes destroy an average of $5 billion in property annually (Pielke and Landsea 1998), largely through wind damage to structures. Hurricane winds and seas are also direct hazards to mariners. Wind does not, however, pose an overwhelming threat to life. Between 1970 and 1999, wind (including hurricane-initiated tornadoes) caused only 16% of hurricane deaths; whereas drowning caused 82%. About a quarter of the drowning deaths were claimed by the wind-driven storm surge. Thus, wind and saltwater forced on shore by the wind combine to cause $<$40% of the U.S. hurricane-related mortality (Rappaport 2000). Still, freshwater flooding due to tropical cyclone rains can cause catastrophic mortality, particularly in developing countries (Pielke et al. 2003). Despite the favorable U.S. experience, storm surge has historically been the greatest killer and remains a potential cause for future large loss of life even in places like the developed shores of North America that have escaped the most lethal effects of tropical cyclones for decades.

2. Parametric profiles

Damaging hurricane winds are generally confined within 100 km of the cyclone center. The wind is calm at the center of the eye. It increases rapidly with radius, reaching a maximum at the outer edge of the cloud-free

Corresponding author address and current affiliation: H. E. Willoughby, International Hurricane Research Center, 360 MARC Building, University Park Campus, Florida International University, Miami, FL 33199.
E-mail: hugh.willoughby@fiu.edu

eye. Outside the eye, the wind decreases with radius, not always monotonically, and approaches zero at several hundred to 1000 km from the center. An early analytical model of the axisymmetric vortex (Riehl 1963) postulated a linear increase (''solid rotation'') outward from the central stagnation point and an inverse power law, with exponent ~0.5, beyond the radius of maximum wind. This model had some observational support (Gray and Shea 1973), but it did not permit calculation of a relation between the maximum wind and minimum sea level pressure because the radial integral of the gradient wind acceleration was unbounded at large radius.

Schloemer (1954) proposed an alternative model for the radial variation of hurricane pressure and the gradient-balance wind computed from it. From this model, Myers (1957) derived a pressure–wind relation in which the maximum balanced wind is proportional to the square root of the pressure difference between large radius and the center of the vortex. In the Schloemer model, the wind distribution was scaled by only two parameters: the maximum wind, $V_{\max}$, and the radius at which the maximum wind occurred, $R_{\max}$. Holland (1980) added a third parameter B, which controls the radial width of the wind maximum. This three-parameter ($V_{\max}$, $R_{\max}$, and B) profile is used extensively to represent the radial distribution of the axisymmetric hurricane winds. Cast in terms of geopotential height of an isobaric surface instead of surface pressure, the Holland mass distribution is

$$z(r) = Z_c + (Z_e - Z_c) \exp[-(R_{\max}/r)^B]. \quad (1)$$

Here, $z(r)$ is the geopotential height of the isobaric surface; Z_e is $z(\infty)$, the height far from the cyclone center and Z_c is $z(0)$, the height at the vortex center. The Schloemer profile is a special case of the Holland profile with $B = 1$. The cyclostrophic wind calculated from (1) is

$$v_c(r) = \sqrt{gB(Z_e - Z_c)(R_{\max}/r)^B \exp[-(R_{\max}/r)^B]}, \quad (2)$$

where g is the gravitational acceleration. As Holland demonstrated, $v_c(R_{\max}) \cong V_{\max}$, so that the cyclostrophic height–wind relation is

$$V_{\max} = \sqrt{gB(Z_e - Z_c)e^{-1}}, \quad (3)$$

and (2) may be recast as

$$v_c(r) = V_{\max}\sqrt{(R_{\max}/r)^B \exp[1 - (R_{\max}/r)^B]}. \quad (4)$$

When the radial and vertical accelerations are small, the wind may be approximated by the gradient wind (Willoughby 1990b) based upon (4).

Figure 1 illustrates the role of B in shaping the wind profile at fixed latitude, $V_{\max}$ and $R_{\max}$. As B increases, the strong winds become increasingly localized near the radius of maximum winds. For larger B, the wind drops off more abruptly both outside and inside the radius of maximum wind, and a larger area of nearly calm wind occupies the vortex center. A key consequence of the variations in profile shape with fixed $V_{\max}$ is a larger geopotential height difference from the vortex periphery to center for smaller values of B. As shown in the appendix, only if all hurricanes could be characterized by the same value of B so that all profiles scaled by $V_{\max}$ and $R_{\max}$ alone, would one expect a universal pressure–wind relation to exist. Contrary to recent analysis by Callaghan and Smith (1998), it is not the size of the vortex, but the shape of the wind profile that determines the pressure–wind relation—apart from a small term proportional to the inverse Rossby number at the radius of maximum wind.

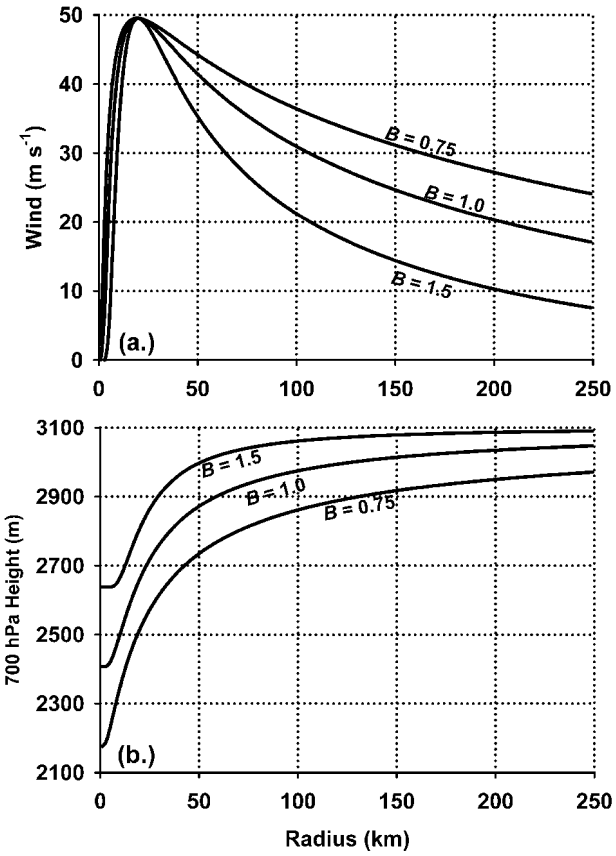

FIG. 1. (a) Gradient winds and (b) 700-hPa geopotential heights computed from the Holland profile at 20° latitude with 50 m s^{-1} max winds at 20-km radius and $B = 0.75$, 1.0, and 1.5.

The Holland profile, combined with climatological data (e.g., Ho et al. 1987), forms the basis of ''catastrophe'' models (e.g., Vickery and Twisdale 1995) used to evaluate insurance underwriting risk. The Schloemer profile provides wind input to the Sea, Lake and Overland Surges from Hurricanes (SLOSH) storm-surge model (Jelesnianski 1967; Jarvinen and Lawrence 1985) and to models of wind-driven seas and other oceanic responses to hurricanes (e.g., Thompson and Cardone 1996). Since these models support decisions where lives and substantial property are at risk, it is reasonable to turn to observations to evaluate the statistics of their

wind-profile parameters and to assess the realism of the wind specification that they provide.

3. Observations

In the late 1970s, the National Oceanic and Atmospheric Administration (NOAA) procured two WP-3D research aircraft, intended to conduct hurricane modification experiments (Willoughby et al. 1985). Although NOAA abandoned weather modification in the early 1980s, these aircraft have provided the Hurricane Research Division (HRD) of NOAA's Atlantic Oceanographic and Meteorological Laboratory with a formidable capability to observe tropical cyclone structure (e.g., Jorgensen 1984a,b; Burpee et al. 1994; Black et al. 2002). From 1977 to the present, a continuing theme of HRD's observational program has been analysis of the structure and temporal evolution of the axisymmetric hurricane vortex (Willoughby et al. 1982; Willoughby 1990a). Starting in 1991, NOAA P-3 observations were augmented by WC-130 missions flown by the 53d Weather Reconnaissance Squadron of the U.S. Air Force Reserve to support operational forecasts, greatly expanding the number of archived cases.

In the flights described here, the aircraft traversed the vortex repeatedly, generally within 150 km of the center. The flight tracks were distributed in azimuth and time to provide a representative sample of vortex structure based upon flight-level measurements of wind and thermodynamic quantities. The storm center locations and motion were determined using the method of Willoughby and Chelmow (1982), and the observations were interpolated into translating, storm-centered cylindrical coordinates. The coordinate change included vector subtraction of the storm motion from the flow to produce storm-relative winds.

This analysis considers wind and geopotential heights of standard isobaric surfaces averaged azimuthally to produce an estimate of the structure of the azimuthal-mean hurricane vortex. The basic unit of analysis is the ''logical sortie,'' a series of consecutive radial penetrations or exits from the eye, uniformly distributed around the vortex at a fixed isobaric level and usually, but not always, flown by one aircraft. The analysis presented here contains 606 logical sorties, observed from 1977 through 2000. Of these sorties, 493 passed quality control (QC) screening. The 113 excluded sorties were compromised by at least one of the following characteristics: (a) radius of maximum wind greater than half of the average radial extent of the sampling domain, (b) minimum winds near the center greater than half the maximum wind, or (c) average minimum distance of the aircraft's closest approach to the center greater than half of the radius of maximum wind. The rationale behind criterion a is the need for enough data outside the eyewall to represent the shape of the wind profile. The rationales behind criteria b and c reflect requirements both for representation of the profile shape inside the eye and for accurate center location to effect the transformation into storm-relative cylindrical coordinates. Criterion a is by far the most common reason for failure to pass QC.

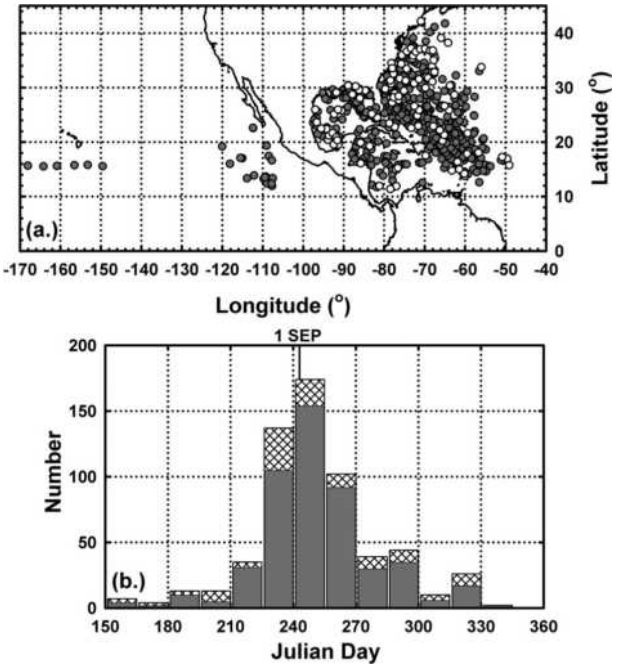

FIG. 2. (a) Geographic and (b) seasonal distributions of observations in the complete flight-level database. Observations that passed quality control (QC) screening (gray-filled circles and bars), those that failed QC (open circles and cross-hatched bars).

Because the database contains many flights carried out under disparate experimental designs over a span of 23 hurricane seasons, it accurately represents both geographical (Fig. 2a) and seasonal (Fig. 2b) hurricane climatology (Neumann et al. 1999). The whole-sample average position is 24.5°N and 76.8°W, near the north end of Exuma Sound in the Commonwealth of the Bahamas, and the average date was 9 September, essentially coincident with the climatological peak in Atlantic hurricane activity. Most (82%) of the observations were taken in the 1990s because of the large contribution from U.S. Air Force Reserve reconnaissance flights (Fig. 3a). For similar reasons, the most common (71%) flight levels are the standard reconnaissance levels (Fig. 3b), 850 and 700 hPa (1.5 and 3 km). Flight crews preferred these altitudes because they were high enough to avoid near-surface, shear-generated turbulence and low enough to avoid airframe icing. Until the late 1990s, 850 and 700 hPa were thought to be the altitudes where the strongest winds occurred. Since then, dropsonde observations (Franklin et al. 2003) have clearly shown that maximum winds in the eyewall are lower, near 500-m altitude. Missions flown below 850 hPa are either reconnaissance sorties into developing tropical depressions or storms (''investigative missions'') or research missions designed to observe the near-surface boundary layer. Ex-

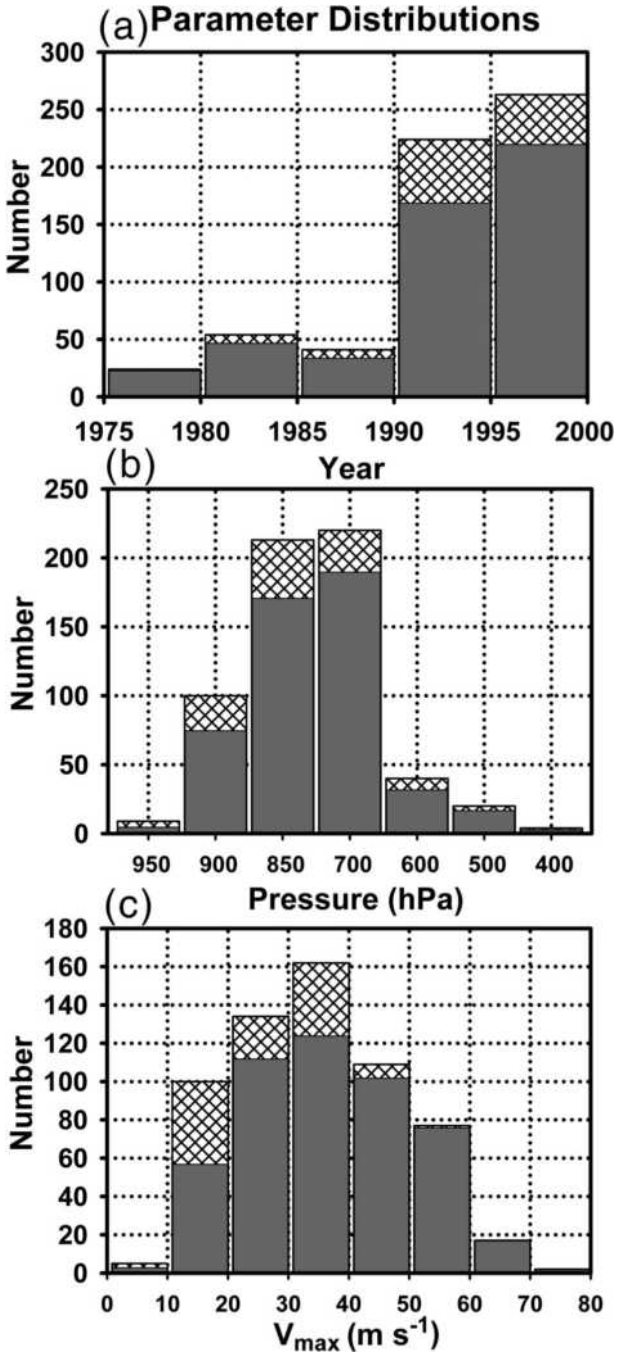

FIG. 3. Histograms of observations in the flight-level database as functions of (a) 5-yr interval during which the observations were made, (b) pressure level where the aircraft flew, and (c) intensity as measured max azimuthally averaged tangential flight-level wind. Filled and cross-hatched bars, respectively, denote observations that passed and failed the QC screening.

perience has shown that very low altitudes are unsafe for WC-130s and P-3s because turboprop airplanes have relatively rigid structure and fly at high true airspeeds. When the NOAA P-3s flew at altitudes other than 850 and 700 hPa, the choice reflected either specific experimental designs or the requirement for altitude separation from Air Force WC-130s operating simultaneously in the cyclone.

The maximum winds in this sample represent a different measure of intensity from those tabulated in the North Atlantic Hurricane Database (HURDAT) ''best track'' files (Jarvinen et al. 1984) maintained by the National Hurricane Center. They are maximum azimuthally averaged winds at several kilometers altitude, whereas HURDAT contains maximum 1-min averaged winds at 10-m elevation anywhere in the storm. The average maximum flight-level wind for the entire sample is 34.6 m s^{-1}, just above the threshold of hurricane intensity. The histogram of intensity (Fig. 3c) is skewed with a tail on the high-intensity side of this mean. Tropical cyclones with maximum wind $<$33 m s^{-1} represented 48% both of sorties in the entire sample and of U.S. landfalling tropical cyclones between 1925 and 1995 (Pielke and Landsea 1998). They also composed 42% of the sorties that passed QC. Thus, despite the tendencies for research missions to target intense hurricanes and for weaker tropical cyclones to fail QC, the sample distribution of intensities seems reasonably representative.

The dataset lends itself to natural partitioning (Table 1) into subsets that represent tropical cyclones in the Atlantic only, those in the Pacific only, those that passed QC, those in the Atlantic that passed QC, and those that failed QC. Compared with the complete data, the Pacific subset (5.6%) was 10° closer to the equator, stronger by 7–8 m s^{-1}, and had mean eye radius of about half the complete-sample average. This bias arose because during seasons when Atlantic hurricanes were suppressed by ENSO (e.g., Gray 1984), NOAA flew research missions in the eastern Pacific to address experimental designs that generally required $V_{max} > 50$ m s^{-1}. The subset that failed the QC (18.6%, all in the Atlantic) was 9 m s^{-1} weaker than the complete-sample average, and had average R_{max} twice as large. This bias arose because, as shown later, there is a negative correlation between V_{max} and R_{max}, and the most common reason for cyclones to fail QC was $R_{max} >$ half the sampling domain size. Nonetheless, the sample was so large that the means and standard deviations were reasonably stable for the subsets that contained $>$400 cases. These were the whole sample, all cyclones that passed QC, all Atlantic cyclones, and Atlantic cyclones that passed QC. For this reason, subsequent statistical analyses use the largest practicable samples and do not draw distinctions among the subsets.

Since the complete sample contains V_{max} and Z_c for all 606 cases, it has enough data to derive an empirical height–wind relationship, given reasonable estimates of Z_e. Mean soundings for the West Indies (Jordan 1958) and in the environments of Atlantic hurricanes (Sheets 1969) provide climatological estimates of the ambient geopotential height $Z_a \cong Z_e$ as a function of pressure that agree well with each other. A scatter diagram of

TABLE 1. Mean maximum wind, radius of maximum wind, latitude, longitude, and Julian day for the different stratifications of the flight-level database.

	No.	V_{max}	R_{max}	Lat	Lon	JD
Complete sample	606	34.59	58.30	24.47	−76.80	251
Atlantic	572	34.10	59.96	24.99	−74.25	251
Pacific	34	42.83	30.30	15.62	−119.71	254
All, passed QC	493	36.70	45.07	23.90	−77.12	252
Atlantic, passed QC	459	36.24	46.16	24.51	−73.97	252
Failed QC	113	25.41	116.00	26.93	−75.41	249

V_{max} as a function of $(Z_a - Z_c)$ for all pressure levels (Fig. 4) shows increasing wind with greater height differences for 604 cases, excluding the two sorties in which the measured central height was greater than the climatological environmental height. A least squares fit of maximum wind to the square root of the height difference is

$$V_{max} = 2.10\sqrt{Z_a - Z_c}. \quad (5)$$

The coefficient in (5) is equivalent to $B = 1.22$ in (3). This fit overestimates wind speed in tropical depression and storms and underestimates the wind in strong hurricanes. Averaged over the entire sample, the fitted curve overestimates the wind by 0.5 m s^{-1} with an rms error of 5.85 m s^{-1}, about two-thirds of a Saffir–Simpson category. The scatter about the best-fit curve appears to be somewhat less than that shown in a similar plot by Shea and Gray (1973) because the azimuthal averaging suppresses larger fluctuations. Sorties that failed to meet the QC criteria are more likely to lie below the curve defined by (5) than above it.

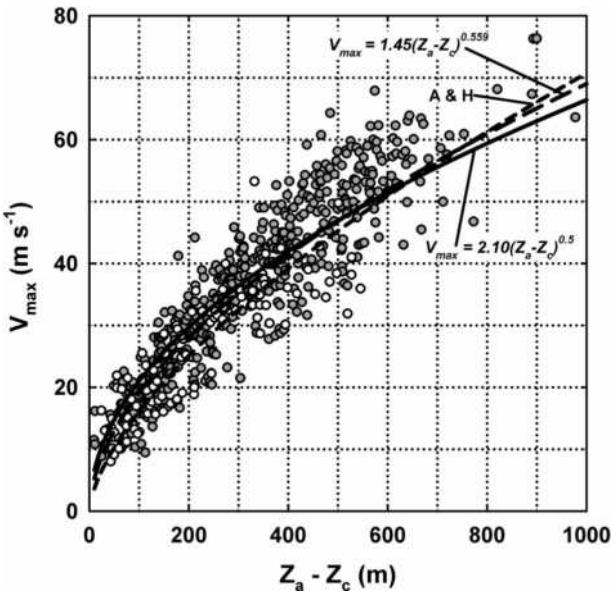

FIG. 4. Empirical height–wind relations calculated from the complete dataset: solid curve denotes max wind proportional to the square root of the geopotential height fall (5), bias and rms error = 0.50 ± 5.85 m s^{-1}; the long-dashed curve denotes power-law curve with variable exponent (6) fitted to the same data, bias and rms error = 0.65 ± 5.67 m s^{-1}; and short-dashed curve represents the Atkinson and Holiday relation between max surface wind and central surface pressure, scaled in terms of geopotential height, bias and rms error = −2.97 ± 6.28 m s^{-1}. Filled and open circles, respectively, mark sorties that passed and failed QC screening.

By way of comparison, Atkinson and Holliday's (1977, hereafter AH) pressure–wind relation, expressed in terms of SI units and geopotential height instead of pressure, is $V_{max} = 0.827(Z_a - Z_c)^{0.644}$. Despite differences between the equations, the height–wind curves computed from (5) and the AH relation are surprisingly similar (Fig. 4). When validated against the flight-level data, AH underestimates V_{max} by nearly 3 m s^{-1} and has rms error >6 m s^{-1}. It is important to recall that AH relates peak 1-min, earth-relative, 10-m winds to minimum sea level pressure in typhoons, but (5) relates azimuthally averaged, storm-relative, flight-level winds to minimum isobaric height in hurricanes. An equation similar to AH fitted to the flight-level data is

$$V_{max} = 1.452(Z_a - Z_c)^{0.559}. \quad (6)$$

The coefficient and exponent in (6) are between those in AH and (5), and the curve lies between them, but closer to the square root relation. Equation (6) has a slightly larger bias error than (5), 0.65 m s^{-1}, but a smaller rms error, 5.67 m s^{-1}. The residual errors after approximation using (5) are skewed toward high values, but on a log–log plot (not shown) the residuals after approximation with (6) are much more symmetric. This situation suggests that the errors may be lognormally distributed and that a variable exponent power-law equation may be more appropriate despite the mixed error statistics.

4. Parameter distributions

a. Radius of maximum wind

Radius of maximum wind is a key parameter that determines spatial scales of hurricane vortices in (1) and (4). Although the Atlantic best-track file (Jarvinen et al. 1984) represents intensity and position of hurricanes that occurred since the late nineteenth century, it contains no information about R_{max}. There is also a general tendency for more intense hurricanes or those in lower latitudes to have smaller eyes, and conversely (e.g., Shea and Gray 1973). A histogram representing the frequency distribution of R_{max} exhibits a substantial tail on the large-radius side of the mean (Fig. 5a), suggesting that

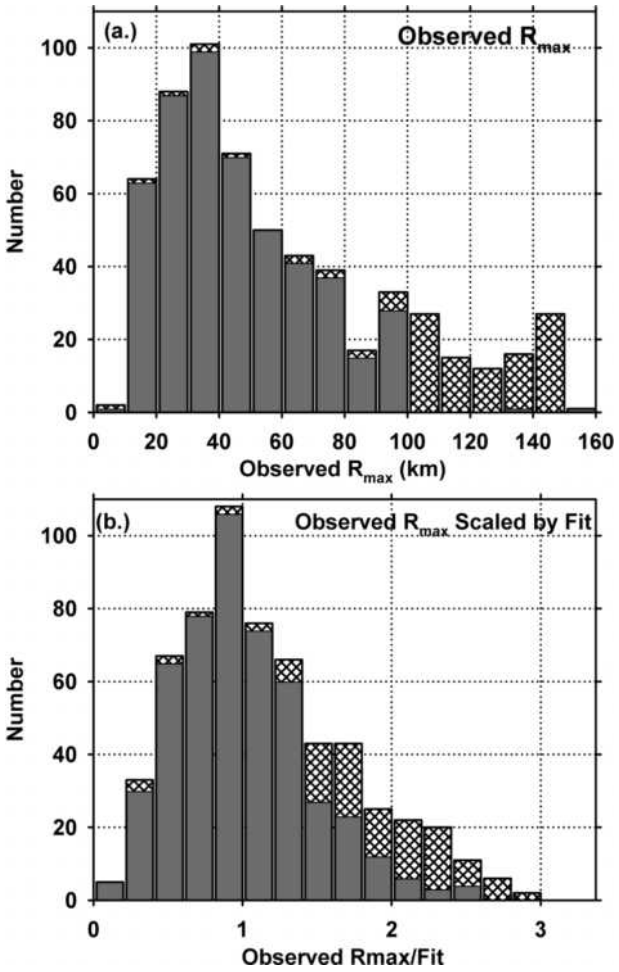

FIG. 5. Histogram of radius of max wind (a) as observed, and (b) divided by the logarithmic least squares fit to the data (8). Filled and cross-hatched bars, respectively, denote observations that passed and failed QC screening.

the $\ln(R_{max})$ may be a more appropriate dependent variable. The geometric mean radius of maximum wind for the complete sample is 47.5 km with logarithmic standard deviation of 0.66, equivalent to variations of between 0.52 and 1.93 times the mean.

Even though most of the cyclones in the tail of the distribution with $R_{max} > 100$ km failed to meet QC criterion a, this limitation does not preclude use of the data to compute a least squares fit (Fig. 6) of the natural logarithm of the radius of maximum wind to maximum wind and latitude, φ:

$$R_{max} = 51.6 \exp(-0.0223V_{max} + 0.0281\varphi), \quad (7)$$

which explains 24.3% of the nonlogarithmic variance and is significant at <1%. Because the range of maximum wind is nearly twice that of latitude, V_{max} contributes more to the variation of radius of maximum wind than φ does. Scaling of R_{max} by (7) narrows the distribution (Fig. 5b), reducing the logarithmic standard deviation to 0.55, which corresponds to variations between 0.58 and 1.73 times the values on the fitted curve. A linear fit to the same data explains more of the nonlogarithmic variance, 28.6%, and is also significant at better than 1%, but leads to the possibility of negative values of R_{max} for statistical fluctuations of less than a standard deviation below the fit for intense hurricanes in low latitudes. A key advantage of the logarithmic fit is that deviations are expressed in terms of ratios rather than sums and differences, so that negative values of R_{max} can never arise. Although the fitted radius of maximum wind in the complete sample decreases significantly with increasing wind speed and increases significantly with latitude, >75% of the variance is random and independent of these quantities. The distribution of residuals remaining after removal of fitted estimates of R_{max} is still skewed toward large values, consistent with a lognormal distribution (Fig. 5b).

b. Holland B parameter

Determination of the properties of the Holland B parameter is more complicated than analysis of R_{max}. It involves fitting the Holland profile to the 493 sorties that passed the QC criteria, followed by statistical analysis of the resulting values of B, which are statistically correlated with R_{max}, V_{max}, and φ. The fit to each observed profile is accomplished by finding the value of B that minimizes a quadratic cost function, S^2, for that profile. The value S^2 is proportional to the sum of the squared differences between v_o and z_o, the observed winds and geopotential heights, and the corresponding Holland-profile gradient winds and heights as functions of B, R_{max}, V_{max}, and φ described by (1), (3), and (4). Maximum wind and radius of maximum wind are readily determined by scanning through each wind profile, and latitude is part of the metadata. The cost function for the minimization is

$$S^2 = \sum_{k=1}^{K} \{[v_o(r_k) - v_g(r_k, B)]^2 + g[z_o(r_k) - z(r_k, B)]^2 L_z^{-1}\}, \quad (8)$$

where the sum is computed over the K radii that have values of wind and geopotential height in each observed profile. The fitted-profile geopotential height is anchored to the observed minimum height at the vortex center, Z_c, so that the environmental height can be computed by solution of (3) for Z_e given knowledge of B and V_{max}. For each profile, B is adjusted using a one-dimensional golden section search (Press et al. 1986) to find the value that produces minimum S^2. Both terms in (8) have dimensions of velocity squared. The value L_z^{-1} is the inverse of a Lagrange multiplier with dimensions of length. It makes (8) dimensionally homogeneous and adjusts the relative importance the wind and geopotential height in the curve fitting. When L_z is small, the geopotential-height term controls the fit; when L_z is large, the wind speed term does.

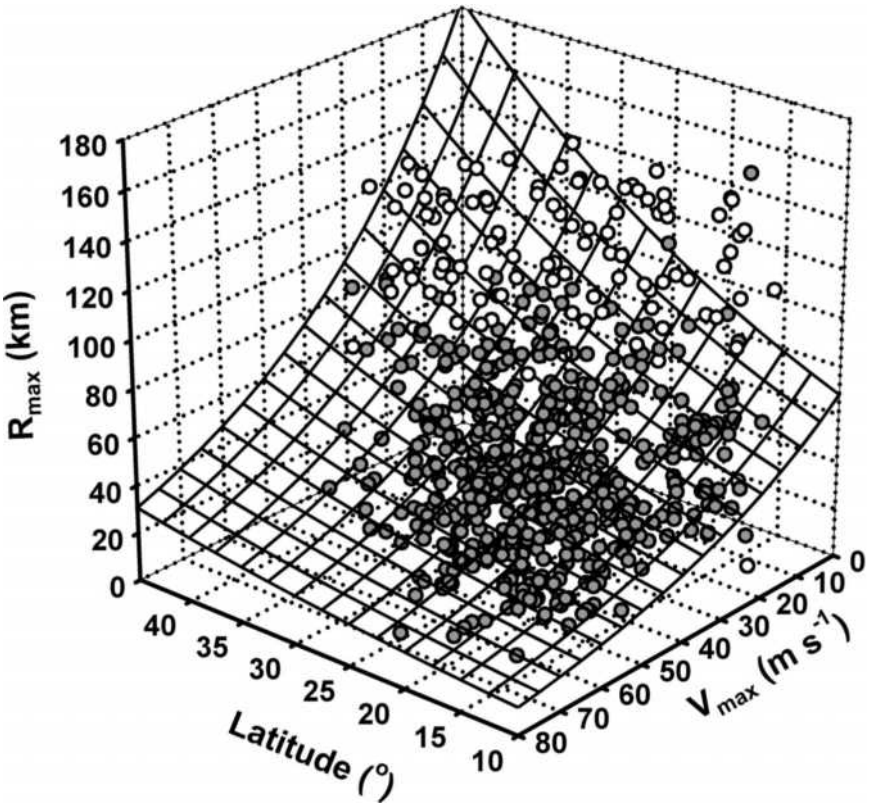

FIG. 6. Logarithmic fit (7) to radius of max wind as a function of max wind and latitude. The gridded surface is the fit. Filled and open circles, respectively, mark sorties that passed and failed QC screening.

Intuitively, one might expect an optimum value of L_z to be comparable with the equivalent depth for hydrostatic wave propagation in the atmosphere—a few hundred meters to a few kilometers. Values in this range imply approximately equal partition between the profile kinetic and available potential energy. Still, there remains the question of what is meant by ''optimum.'' By design, changes in L_z exert some control over the fitted width parameter. The sample mean B is 1.39 at L_z = 250 m. It decreases to 1.31 at L_z = 1 km, and then approaches a value of about 1.25 as L_z increases to 4 km (Fig. 7a). Since the standard deviation of B at L_z = 1 km is 0.36, the 0.14 systematic change is relatively small compared with the random variation. It seems reasonable to require the averages of the environmental heights (Z_e) computed from (3) for all the sorties at each isobaric level to be close to the climatological environmental height for that level (Z_a), and at the same time to strike a compromise between the simultaneous decrease of wind rms errors and increase of geopotential-height rms errors with increasing L_z. The sample average ($Z_e - Z_a$) is -14 m when L_z = 250 m (Fig. 7b). It remains negative for $L_z < 900$ m. At larger values of L_z, the difference becomes positive, increasing to >16 m for L_z = 4 km. The rms wind error is 5 m s^{-1} at L_z = 250 m. It decreases to 4.27 at L_z = 1 km and then approaches a value <4 m s^{-1} asymptotically as L_z increases to 4 km (Fig. 7c). The wind bias error increases from -1.23 m s^{-1} to zero over 250 m $\leq L_z \leq$ 4 km, again with most of the increase between 250 m and 1 km. The bias is -0.52 m s^{-1} when L_z = 1 km. The geopotential-height bias and rms errors increase monotonically as the gradient-balance constraint relaxes with increasing L_z. They are 2.3 and 12 m, respectively, when L_z = 250 m, increasing to 9.8 and 20 m when L_z = 1 km and then to 17 and 32 m when L_z = 4 km. Thus, L_z = 1 km seems to be the best compromise value, because B and the wind errors do not change much for $L_z \geq$ 1 km, the computed and climatological environmental heights agree, and the geopotential height errors are acceptable.

Hurricane Anita of 1977, chronologically the first profile in the database, illustrates some of the characteristics of the fitted profiles. The central area of calm winds is much broader in the fitted wind profile than in the observations (Fig. 8a). The wind maximum in the Holland profile is also broader; so that the profile wind is stronger than the observed wind between 10- and 50-km radius, except at R_{max} where it is constrained to be the observed V_{max}. Beyond r = 50 km, the fitted-profile wind is weaker than the observed wind, and the difference increases with increasing r.

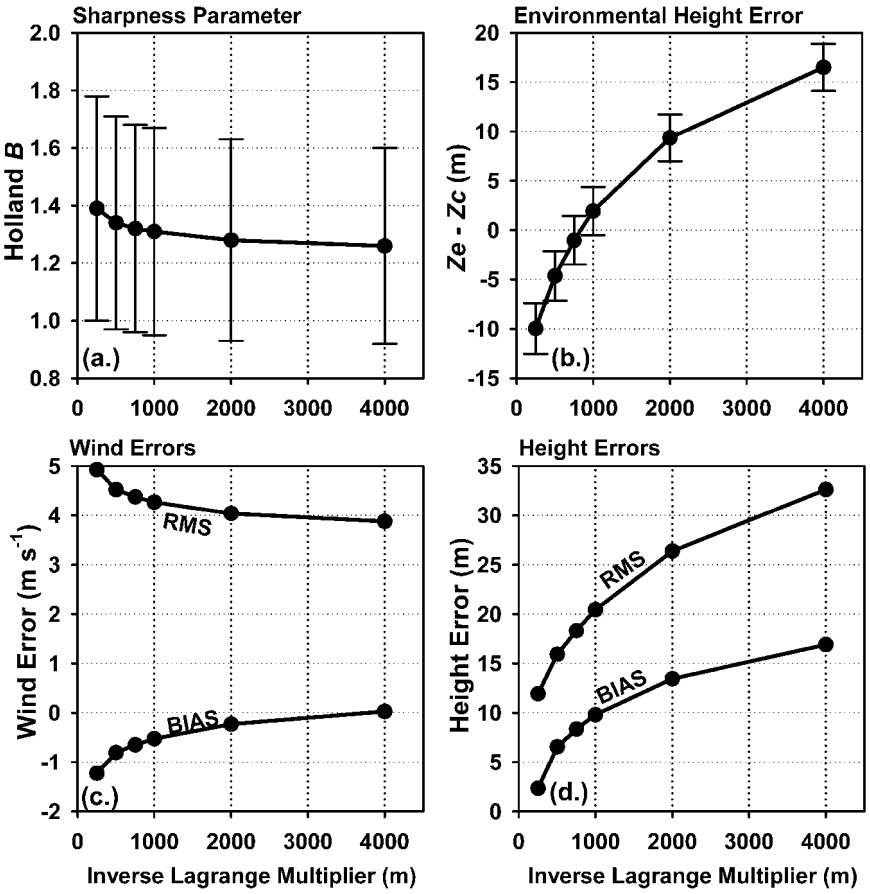

FIG. 7. The effect of the gradient-balance constraint on the Holland profile fit: (a) variations of sharpness parameter, (b) difference between the calculated and climatological environmental height, (c) wind rms and bias errors, and (d) geopotential-height rms and bias errors.

The wind errors cause errors in the balanced height field. At the center of the vortex, the fitted geopotential height is constrained to be the observed minimum, Z_c. Because the Holland-profile winds are weaker than the observed winds within 10 km of the center, the profile geopotential height increases too slowly outward from the center to about ½ R_{max}. In the eyewall, where the fitted wind is significantly stronger than the actual wind, the fitted height increases too rapidly so that it becomes greater than the observed height by 25-km radius. This positive bias results in an overestimate of the geopotential height that persists outward to the edge of the domain. Beyond $r = 50$ km where the observed wind again exceeds the fitted wind, the height bias decreases slowly with increasing radius. This pattern of wind and height errors, which is typical of the data as a whole, highlights the limitations of the Holland profile for many applications.

The systematic errors also explain the way that the gradient-wind constraint changes the statistical properties of the fit. The larger values of B for smaller L_z in Fig. 7a arise because the penalty due to the positive height bias outside the wind maximum forces the fitting algorithm to sharpen the maximum. This effect also increases the rms and negative bias wind errors by causing the wind to decrease more rapidly with radius outside the eye. Conversely, for larger values of L_z, the wind maximum is broader because the algorithm selects smaller B; the resulting wind rms and bias errors are also a bit smaller at the expense of larger height errors. When $L_z = 1$ km, the small average difference between calculated and climatologically expected Z_e arises from compensation between the gradient wind relation's overestimate of the geopotential-height gradient near the too-broad wind maximum and its underestimate of the geopotential-height gradient in the too-weak wind in the outer vortex.

The pattern of errors identified in Anita appears to a greater or lesser extent in the other profiles. Radial variation of the wind falls into two classes: sharply peaked profiles, as in Mitch of 1998 (Fig. 9a) or Hugo of 1989 (Fig. 9b), which generally occur in intense hurricanes; and broad or relatively flat profiles, as in Edouard of 1996 (Fig. 9c) or Erica of 1997 (Fig. 9d), which generally occur in weaker hurricanes or those that have passed peak intensity. In cases like Mitch and Edouard,

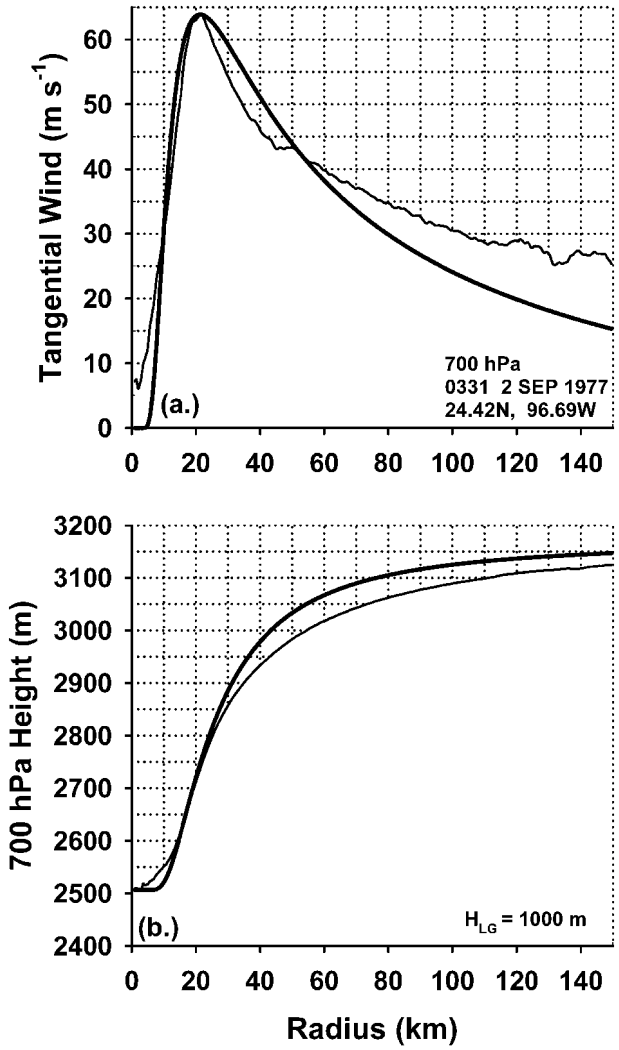

FIG. 8. Fit of the Holland profile to the azimuthal-mean structure of Hurricane Anita on 2 Sep 1977: (a) tangential wind and (b) 700-hPa geopotential height. Here, and in Figs. 9 and 10, the dark smooth curves are the fitted profiles and the lighter curves that bound areas without reference lines represent the observations.

the Holland profile does reasonably well; in others, like Hugo and Erica, it is less successful. The best results occur when the wind maximum is either fairly broad and the actual decrease outside the eye is rapid (Mitch) or the value of $B < 1$ is such that the broad fitted profile matches the observations even far from the center (Edouard). Sharply peaked profiles, however, usually force selection of a large value of B that leads to too-rapid decline of wind with radius (Anita and Hugo) far from the center. In some other cases, the initial scan for V_{max} locks onto an isolated wind maximum on an otherwise flat profile. In these situations, the fitted profile overestimates wind almost everywhere (Erica). Attempts to fix this problem using a three-parameter variational fit to determine R_{max}, V_{max}, and B generally overestimated the radius of maximum wind, underestimated the maximum wind, and smoothed the eyewall structure so much that the fitted and observed profiles were qualitatively different.

Hurricanes with prominent outer wind maxima are unsuited to representation with this model. Hurricane Allen as it approached landfall on the Texas coast produced the fourth-largest rms error in the sample, 12.6 m s^{-1} (Fig. 10a). The sorties with errors larger than this one were also spectacular examples of concentric eyewalls: two in Allen on the previous day and one in Gilbert as it approached landfall on the Yucatan Peninsula. The recurrent pattern of positive height errors due to overestimation of the wind on the flanks of the wind maximum and underestimation of the wind at large radius is overwhelming in this case (Fig. 10b).

The histogram of values of B that result from the profile fits (Fig. 11a) shows a more or less symmetric distribution, somewhat flatter than a normal distribution, and with narrower tails because the minimization algorithm is constrained from finding values outside $0.5 < B < 2.5$. The mean and standard deviation are 1.31 ± 0.36. Experience and the data shows that B varies systematically as a function of $\ln R_{max}$, V_{max}, and φ. The logarithmic transformation of R_{max} reflects the skewed distribution of that variable and consistency with (7). A least squares fit to the 493 sorties in the complete dataset that passed the QC is

$$B = 1.0036 + 0.0173V_{max} - 0.0313 \ln R_{max} + 0.0087\varphi. \quad (9)$$

The coefficients of V_{max}, and φ differ from zero at $<1\%$ significance, but the coefficient of $\ln R_{max}$ is not significant, largely because of the smaller dynamic range of the logarithm and the rejection by the QC of tropical cyclones with large eyes. In an analogous fit where R_{max} enters linearly, the coefficient is nonzero at the 5% level. Nonetheless, we retain the middle term for consistency with both (7) and subsequent discussion of the correlation matrix for the parameters. Three-dimensional plots of (9) and the data (Fig. 12) show that V_{max} is the dominant predictor of B. Subtraction of B computed with (9) from the values of B produced by the profile fits narrows the distribution (Fig. 11b) and reduces the standard deviation from 0.36 to 0.25. The fit explains 51% of the variance.

An alternative statistical representation treats the Holland profile parameters as a vector of the standardized normal random variables:

$$\mathbf{Z} = \begin{vmatrix} Z_1 \\ Z_2 \\ Z_3 \\ Z_4 \end{vmatrix} = \begin{vmatrix} (V_{max} - \overline{V}_{max})/\sigma_V \\ \ln(R_{max}/\overline{R}_{max})/\sigma_R \\ (\varphi - \overline{\varphi})/\sigma_\varphi \\ (B - \overline{B})/\sigma_B \end{vmatrix}, \quad (10)$$

where overbars denote means and the σs are standard deviations, except for R_{max} where $\overline{R}_{max}$ is the geometric mean and σ_R is the logarithmic standard deviation. The

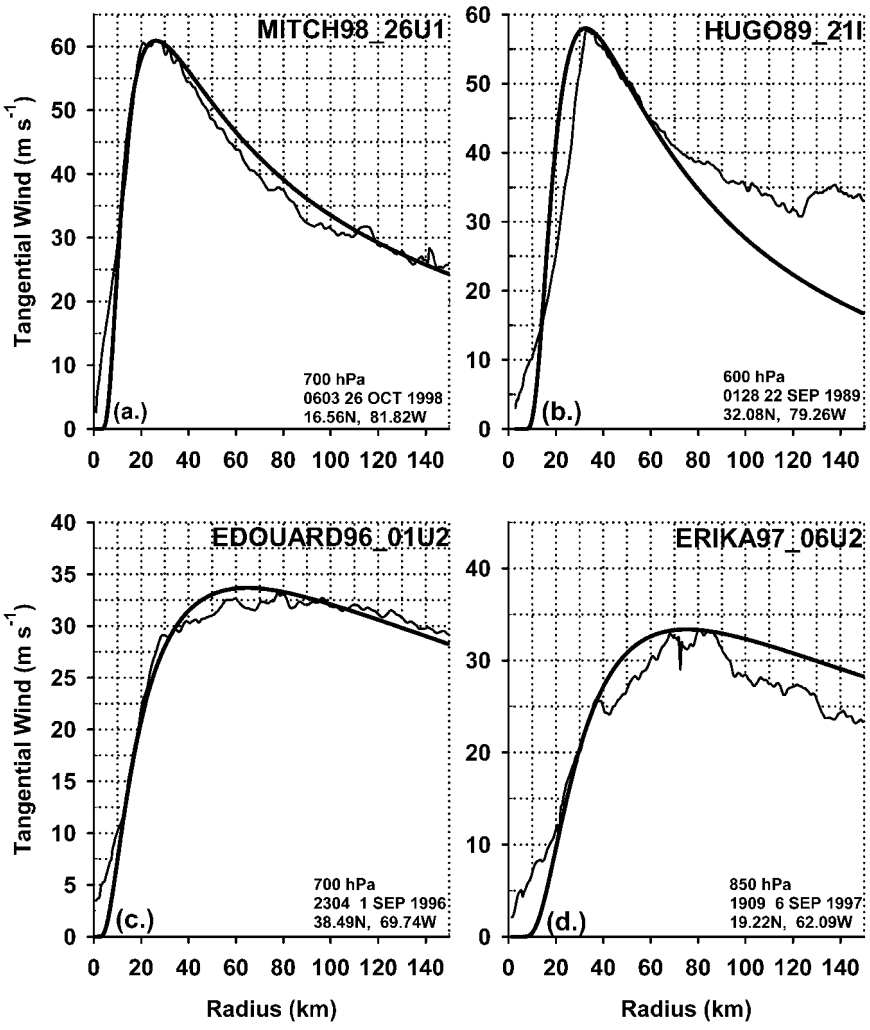

FIG. 9. Examples of the Holland-profile winds fitted to hurricane observations: (a) Hurricane Mitch of 1998, (b) Hurricane Hugo of 1989, (c) Hurricane Edouard of 1996, and (d) Hurricane Erica of 1997. See caption to Fig. 8 for details.

correlation matrix, **C**, of the *Z*s, summed over the sorties that met the QC criteria (Table 2a) shows, not surprisingly, strong positive correlation between $Z_1(V_{\max})$ and $Z_4(B)$, and half as strong negative correlation between $Z_1(V_{\max})$, and $Z_2(\ln R_{\max})$. The other correlations are smaller, consistent with (7) and (9). The total standardized variance of the system is 4.0, the sum of the diagonal elements of **C**. Projections of **C**'s, eigenvectors onto **Z** are consistent with intuition and previous analysis (Table 2b). The leading eigenvector, E1, explains more than half of the standardized variance. As $Z_1(V_{\max})$ increases, E1 projects strongly onto increasing $Z_4(B)$ and decreasing $Z_2(\ln R_{\max})$. This pattern of correlation represents the ''convective ring process,'' contraction of the eye and sharpening of the wind maximum in response to symmetric heating in the eyewall as described by Smith (1981), Shapiro and Willoughby (1982), and Schubert and Hack (1982). Strong positive values of E1 correspond to sharply peaked wind profiles as shown in Figs. 8, 9a and 9b; negative projections to broad profiles as shown in Figs. 9b and 9c, although generally with weaker winds than shown in those figures. The second eigenvector, E2 explains about a quarter of the variance. It projects primarily onto $Z_3(\varphi)$ with a slight decrease in maximum wind at lower latitudes or an increase in maximum wind at higher latitudes, independent of the variation of $R_{\max}$ and B described by E1. The remaining two eigenvectors, E3 and E4 explain only 17% and 7% of the total variance, respectively.

An alternative to the regression analysis leading to (7) and (9) involves formation of a multivariate normal distribution using the correlation matrix:

$$f(\mathbf{Z}) = \frac{\exp\left\{-\frac{1}{2}\mathbf{Z}\mathbf{C}^{-1}\mathbf{Z}\right\}}{4\pi^2\sqrt{|\mathbf{C}|}}. \qquad (11)$$

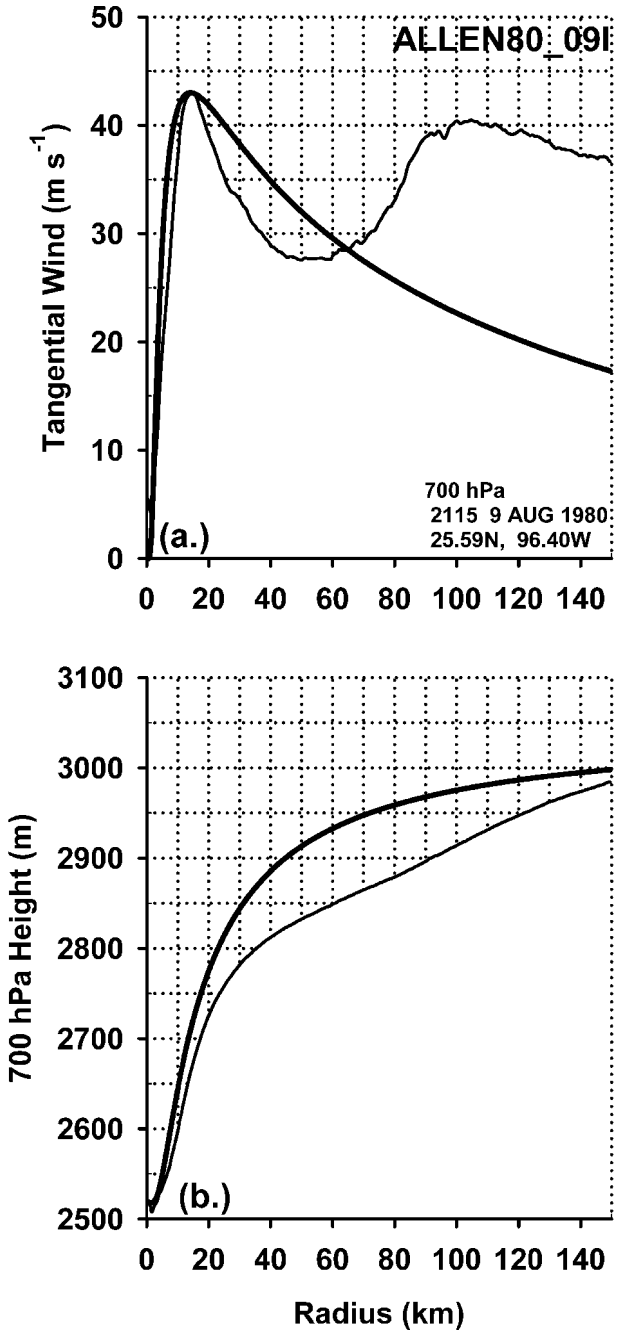

FIG. 10. (a) Swirling wind and (b) 700-hPa geopotential height for one of the least successful fits, the concentric-eyewall profile of Hurricane Allen as it approached the Texas coast on 9 Aug 1980. See caption to Fig. 8 for details.

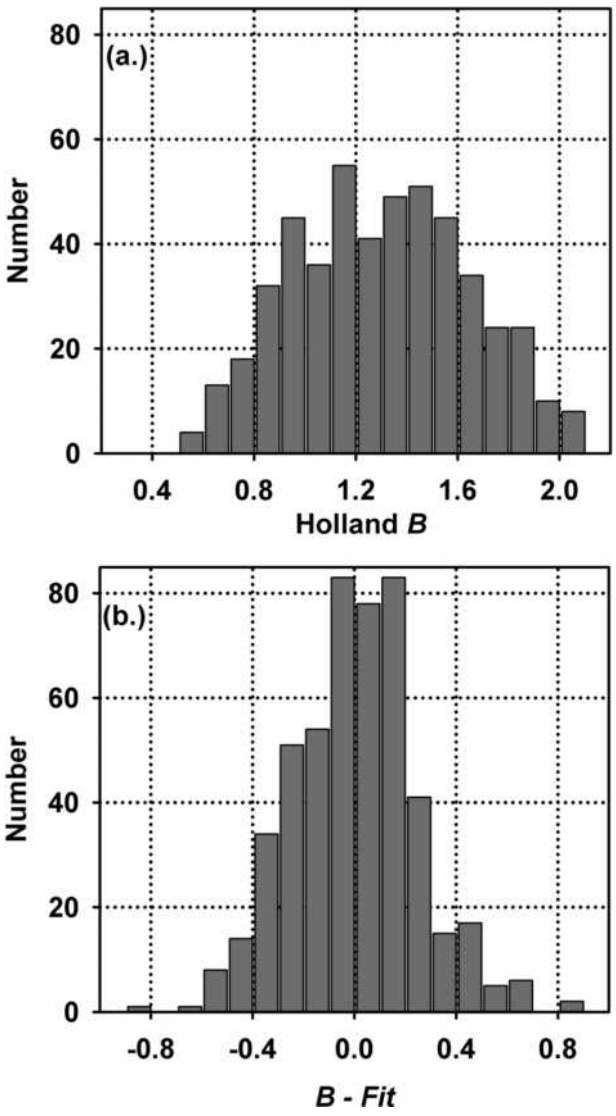

FIG. 11. Histograms of the Holland B parameter (a) as computed by the fitting algorithm for all 493 profiles that passed QC, and (b) with the least squares fit (9) as a function of V_{max}, R_{max} and φ subtracted.

A key advantage of this representation is that, for example, an investigator working with best-track data would know maximum wind and latitude but not radius of maximum wind or B, but could divide (11) by the marginal (standardized bivariate normal) distribution of $Z_1(V_{max})$ and $Z_3(\varphi)$ and substitute the known values of Z_1 and Z_3 to obtain the conditional bivariate standardized normal distribution of $Z_1(V_{max})$ and $Z_4(\ln R_{max})$ centered around a point in **Z** space determined by Z_1 and Z_3 on the regression relation among the standardized variables:

$$R_{max} = 46.29 \exp(-0.0153V_{max} + 0.0166\varphi), \quad (12.1)$$

$$B = 0.886 + 0.0177V_{max} - 0.0094\varphi. \quad (12.2)$$

These relations are identical with the results of convectional least squares fitting of B and R_{max} to V_{max} and φ, but the resulting conditional probability distribution contains measures of correlation and central tendency. The equation for R_{max} (12.1) differs from (7) because it is based only on data that passed QC screening. Limitations of this approach lie in the approximate normality of the parameters, which may cause underestimation of

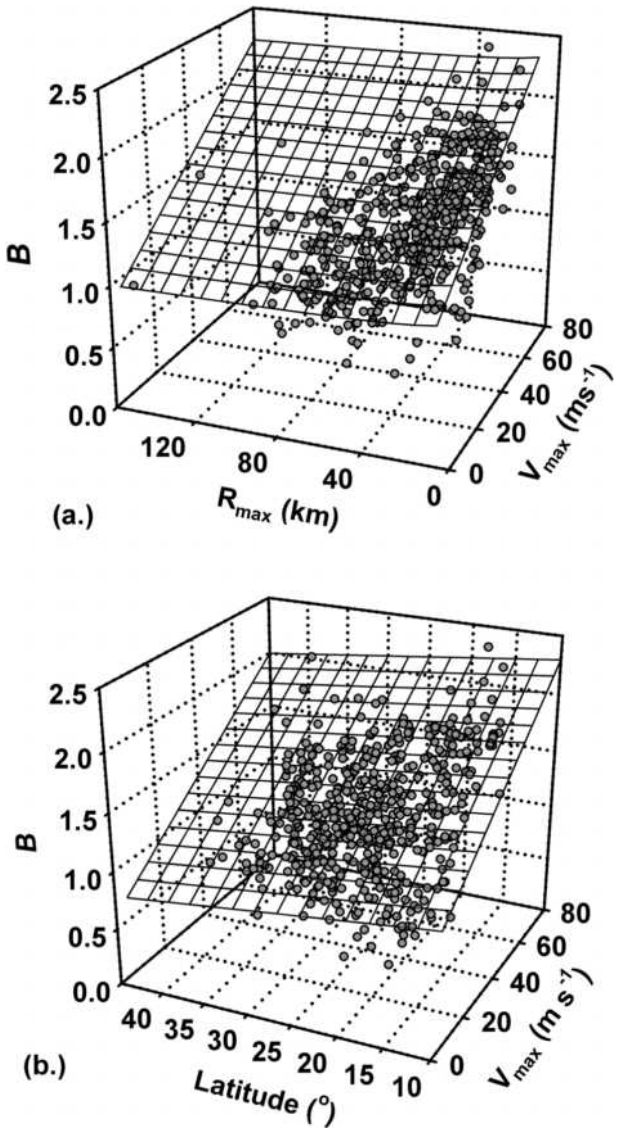

FIG. 12. Data and least squares fit (9) of B to V_{max}, R_{max} and φ. Variations (a) of B as a function of V_{max} and R_{max} and (b) as a function of V_{max}, and φ.

the actual variance, and the exclusion of the sorties that failed QC from calculation of **C**. Since the QC preferentially removed storms with large R_{max}, (12.1) fails to capture the full range of variability of eye size in nature.

The sharpening of the wind maximum due to the increase of B in stronger hurricanes affects the wind–height relationship. Since Table 2a and Fig. 12 show that maximum wind is the parameter most strongly correlated with B, a linear relation between B and the maximum wind is obtained by substituting the mean values of φ and $\ln R_{max}$ into (9) to obtain $B = 0.662(1 + 0.0267 V_{max} = B_0(1 + \gamma V_{max})$ at latitude 23.9°N. This relation is a reasonable way to account for the sharpening of the profile with stronger maximum wind. Substitution into (3), solution of the quadratic equation, and selection of the positive root yields the height–wind relation for variable B:

$$V_{max} = V_0\left[\sqrt{1 + \frac{(\gamma V_0)^2}{4}} + \frac{\gamma V_0}{2}\right], \qquad (13)$$

where $V_0 = \sqrt{gB_0(Z_e - Z_c)e^{-1}} = 1.56\sqrt{Z_e - Z_c}$ is the baseline wind that would result if γ were zero. When compared with the observed values of V_{max} and $(Z_a - Z_c)$, this height–wind relation (Fig. 13) has a consistent bias of nearly 3 m s^{-1} toward strong wind and an rms error more than 6 m s^{-1}, a value greater than the rms error of the empirical height wind relation (Fig. 4). Thus, consistent application of the Holland profile both overestimates the maximum wind and spreads the strongest winds over too widely around the maximum. The reason for the former error lies in underestimation of the wind around the cyclone's center and beyond 2 or 3 times the radius of maximum wind, which leads to underestimation of the total height difference from the large radius to the center, despite the systematic overestimation of the wind on the flanks of the eyewall maximum. By contrast, the height–wind relation computed with the mean B has a bias of -0.86 m s^{-1} and an rms error of 5.96 m s^{-1}.

Safety of flight and experimental design dictated aircraft altitude. With few exceptions, aircraft did not operate below 1.5-km altitude (850 hPa) in hurricane-force winds. In major hurricanes, stronger than 50 m s^{-1}, they almost invariably flew at 3 km (700 hPa). The increase of average wind with height up to 700 hPa in the sample (Fig 14a) thus stems from the reluctance of aircrews to fly at low altitudes in intense tropical cyclones. For a definitive picture of tropical cyclones' lower-tropospheric vertical wind structure one must turn to composites of dropsonde soundings (Franklin et al. 2003). A crucial inconsistency between Fig. 14 and the soundings is that in the soundings the wind maximum in the eyewall is at 500-m altitude, not at 3 km. Above 700 hPa, the decrease in maximum wind in the flight-level data, though consistent with both the expected thermal wind decrease in a warm-core cyclone and the soundings, is not convincing because of the small sample size and large inherent variability of the measurements. Despite the documented outward slope of the eyewall in individual hurricanes (Jorgensen 1984b), the average radius of maximum wind in the present sample (Fig. 14b) decreases from 900 to 700 hPa, consistent with the increase in average intensity of hurricanes flown at the higher altitudes. The decrease in radius of maximum wind above 600 hPa is probably the result of random variations in the small sample. Similar considerations apply to the vertical variation of B. As in the case of R_{max}, the increase of B from 900 to 700 hPa reflects the correlations between B and intensity, whereas above 700 hPa, the observations are too few to support analysis of a convincing trend. Thus, while the observations at hand provide considerable insight into the horizontal structure

TABLE 2. (a) Mean, standard deviation, and correlation matrix for the Holland profile variables computed from the 493 sorties in the entire dataset that passed QC screening. For R_{max} the entries differ from those in Table 1 because they are the geometric mean in kilometers and the logarithmic standard deviation. (b) Eigenvalues and eigenvectors of the correlation matrix.

(a)

	Distribution		Correlation matrix			
	Mean	SD	Z_1	Z_2	Z_3	Z_4
Z_1 (V_{max})	36.7	13.7	1.000	−0.398	−0.018	0.693
Z_2 (ln R_{max})	39.3	0.53	−0.398	1.000	0.200	−0.347
Z_3 (φ)	23.9	6.15	−0.018	0.200	1.000	−0.177
Z_4 (B)	1.31	0.36	0.693	−0.347	−0.177	1.000

(b)

Eigenvector	E1	E2	E3	E4
Eigenvalue	2.024	1.009	0.686	0.281
Z_1 (V_{max})	0.600	0.332	0.162	−0.709
Z_2 (ln R_{max})	−0.480	0.194	0.847	−0.121
Z_3 (φ)	−0.209	0.912	−0.302	0.181
Z_4 (B)	0.605	0.140	0.406	0.670

of hurricanes and tropical storms, overrepresentation of altitudes between 1.5 and 3 km and the strong correlation between preferred flight level and intensity mean that they provide no information about average vertical structure.

5. Verification

All of the statistics presented so far employ dependent data, based upon values of the parameters V_{max}, R_{max}, and B that are chosen uniquely to produce optimum fits to individual observed profiles. Key concerns are statistical robustness and the ability to represent independent data. Here, we address these questions with a ''bootstrap'' technique in which the linear estimates of B and R_{max}, (12.1) and (12.2), are rederived based upon subsets of the data and validated against the complementary subsets. The three data partitions used encompass years: 1977–89 (107 cases, 96 passed QC), 1990–95 (235 cases, 177 passed QC) and 1996–2000 (263 cases, 220 passed QC). In the bootstrap procedure, statistics for each partition are computed using mean or linearly estimated B based upon the other two partitions. For example, the statistics for 1977–89 use statistical models of the parameters based upon the profiles that passed QC in 1990–95 and 1996–2000. In an effort to get more statistical independence, some of the calculations use all profiles in the independent-data partitions, not just those that passed QC. The partition-specific independent-data statistics are then combined in weighted averages to see how representative the entire sample is. Exclusion of the profiles that failed QC from the independent-data partitions decreases the rms errors by 3%–5% and *increases* the bias errors, which remain relatively small, by 15%–30%.

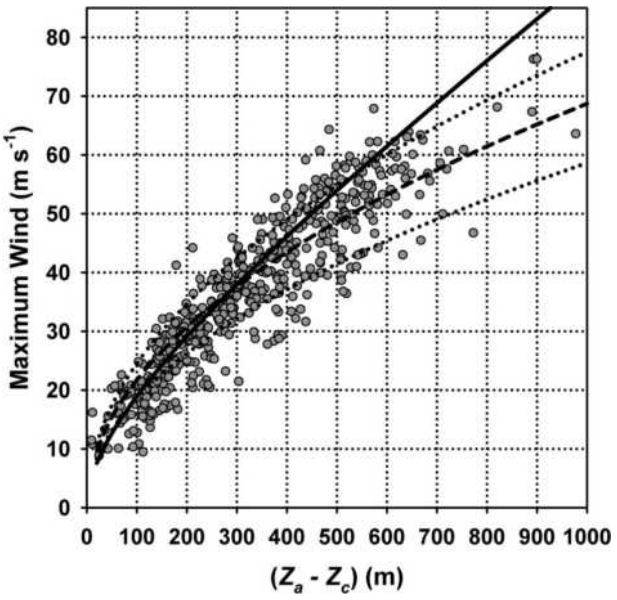

FIG. 13. Height–wind relations hips for the tropical cyclones that passed QC screening, based upon the mean value of B (dashed) plus and minus one std dev (dotted) and B that varies as a function of V_{max}(solid). For the variable-B curve, the bias and rms errors, based upon the 491 sorties that passed QC and had positive $Z_a - Z_c$, was 2.53 ± 6.48 m s^{-1}.

The baselines for comparison with the bootstrap results are -0.52 and 4.27 m s^{-1}, respectively, the bias and rms errors computed in section 4 with dependent-data, profile-specific values of B. Bootstrap wind errors based upon partition-specific versions of (9) and the actual values of R_{max} are a samplewide bias of -0.60 m s^{-1} and an rms error of 5.24 m s^{-1}. If, instead, the sharpness parameter is represented by the constant mean value of B for each bootstrap combination, the bias and rms errors are -0.14 and 5.51 m s^{-1}. Thus, validation against independent data increases the rms error by only about 23% and has negligible effect on the bias. The modest error increase from dependent to independent data substantiates the assertion that the sample is representative. One might not prefer linear variation of B as a function V_{max}, R_{max}, and φ to a simple average value

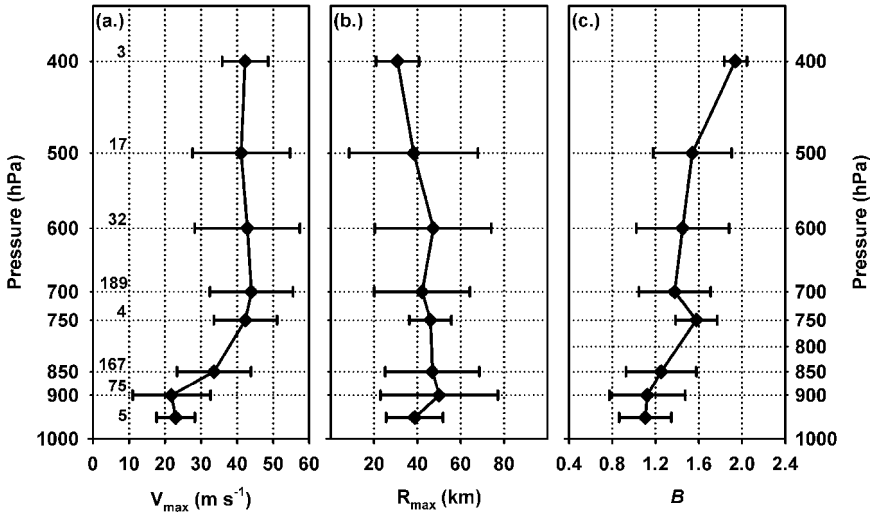

FIG. 14. Variations of (a) max wind, (b) radius of max wind, and (c) Holland *B* parameter as functions of the pressure at flight level.

of *B*—at least if the mean and rms errors are the primary criteria. The slightly smaller errors in the height–wind relation with the average value of *B* compared with that based upon *B* that varies with V_{max} (Fig. 13) are consistent with this statement.

Bootstrap results using linear estimates of both *B* and R_{max} have comparable bias but larger rms error, 0.07 and 7.35 m s^{-1}. With mean *B* and linearly estimated R_{max}, the errors are not much different, and the whole-sample errors are incrementally *smaller* than those computed with only the independent-data profiles that met the QC criteria. The 40% increase in rms error with statistically estimated R_{max} highlights the dependence of the computed wind field on an accurate measure of vortex spatial scale.

Since a primary application of parametric models is stochastic estimation of windstorm risk rather than description of individual storms, any validation scheme needs to consider the statistical distributions of observed and modeled wind values. Figure 15 shows homogeneous-sample, wind-value histograms for the observations, dependent-data fitted profiles, and bootstrap profiles that met the QC criteria with linearly estimated *B* and actual R_{max}. Since the occurrences are not area-weighted they do not translate readily into probabilities. The vertical scale is logarithmic so that agreement between the distributions may appear better than it is. The occurrences peak between 20 and 30 m s^{-1}. Only around the peak do the observed and fitted-profiles occurrences agree. Just above the peak, between 30 and 40 m s^{-1}, the fitted profiles underestimate the wind speed–value occurrences by ~20%. Elsewhere, on the high and low sides of the maximum, the fitted profiles overestimate the occurrences. The problem is particularly severe for winds in the 50–60, 60–70, and 70–80 m s^{-1} ranges where the profiles exaggerate the occurrence by 51%, 76%, and 39%, respectively. Since the dependent-data and bootstrap profiles are more consistent with each other than with observations, the exaggeration stems from the character of the Holland profile rather than the statistical estimation of the parameters.

Similar results arise from a complete-sample comparison among observations, profiles with bootstrap linearly varying *B*, and profiles computed using bootstrap average *B* (Fig. 15b). Despite their acceptable rms error and height–wind relation, the mean-*B* profiles exaggerate the occurrence of high wind speeds even more severely than those with linearly estimated *B* because they fail to capture the narrowing of the eyewall wind maximum in the most intense hurricanes.

6. Conclusions

Data from >600 aircraft sorties into Atlantic and eastern Pacific tropical cyclones provide a geographically and seasonally representative sample of their wind and geopotential height profiles. Of the 606 aircraft sorties in this sample, 493 passed quality control screening designed to ensure that they sampled the vortex uniformly enough to support statistical fits of the Holland (1980) analytical profiles. The Holland profile is characterized by the three parameters: maximum wind, radius of maximum wind, and *B*, which determines the sharpness of the wind maximum. Sample average values of the parameters are, 36.7 m s^{-1}, 45 km (geometric mean = 39.3 km), and 1.31 for the 493 profiles. The leading eigenvector of correlation matrix computed for these parameters and latitude explains more than half of the variance. It shows that radius of maximum wind decreases and *B* increases as maximum wind increases, consistent with the dynamical models of tropical cyclone response to axisymmetric convective heating.

Comparison of the fitted profiles with observations shows a consistent pattern of errors. The fitted profiles

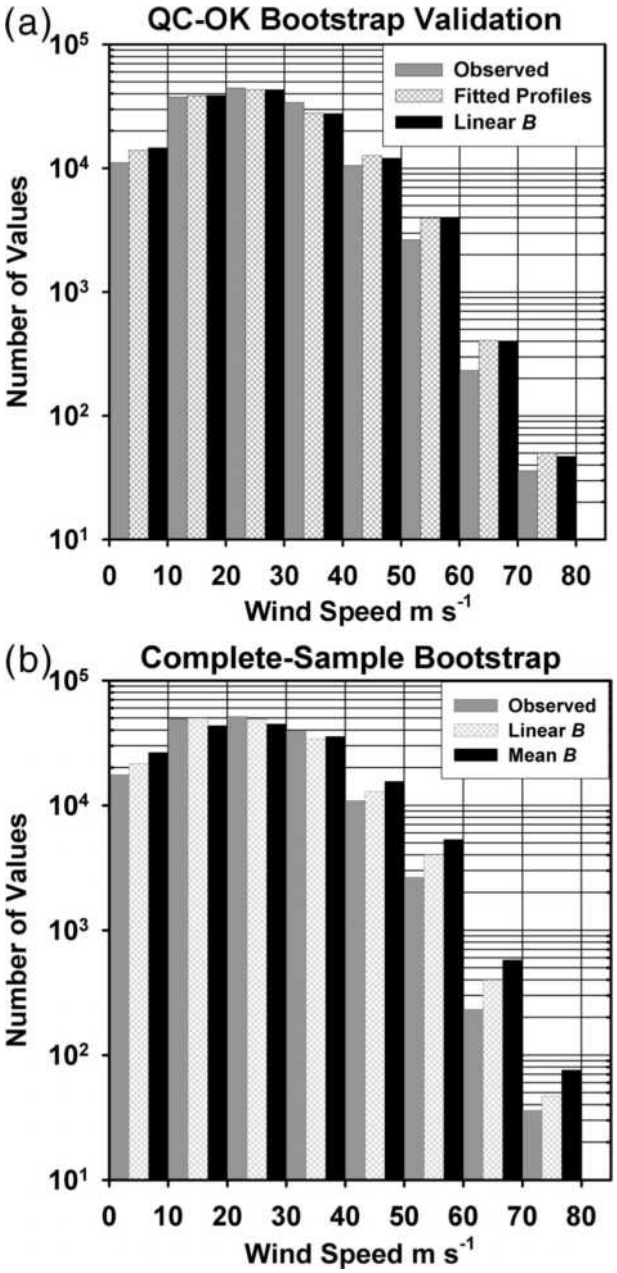

FIG. 15. (a) Histograms of wind speed occurences for the observations (gray), dependent-data fitted Holland profiles (cross hatched), and Holland profiles with bootstrap linear estimates of B (black) for data that met the QC criteria. (b) Complete sample histograms for observed (gray), bootstrap linear B Holland profiles (cross hatched), and bootstrap average B (black). All profiles use actual values of R_{max}.

overestimate the wind on the flanks of the eyewall wind maximum, but away from eyewall they underestimate wind. The central calm is too large, and at radii greater than 2 or 3 times the radius of maximum wind, the wind decreases too rapidly with increasing radius. As a result of these systematic errors, the Holland profile overestimates the occurrence of winds stronger than 50 m s^{-1} by >50%. The height–wind relation (13) based upon the increase of B with V_{max} in the fitted profiles has a 2.5 m s^{-1} bias toward strong winds and an rms error of 6.5 m s^{-1}, equal to 2/3 of a Saffir–Simpson category. These limitations suggest the need for an alternative formulation. In a companion paper we will propose a sectionally continuous parametric profile that avoids the foregoing pitfalls.

Acknowledgments. We are grateful to everyone at NOAA and in the U.S. Air Force who flew and supported the aircraft missions upon which this paper is based. Our admiration for their unfailing professionalism, skill, and dedication to a difficult and demanding undertaking is boundless. HEW began work on this project at the Hurricane Research Division. The acquisition and maintenance of the data archive was supported by HRD base funds. HEW's efforts since December 2002 were supported by Florida International University research discretionary funds. We thank Sneh Gulati for statistical advice and Chris Landsea for insightful comments on an earlier draft.

APPENDIX

Necessary Conditions for a Unique Height–Wind Relation

A family of axisymmetric wind profiles that could be characterized by a single horizontal spatial scale, a single velocity scale, and a universal nondimensional shape function, v', would have a universal height–wind relation. In such profiles, all radial distances are expressed as multiples of R_{max} and all velocities as multiples of V_{max} as was done in the hurricane-scale analysis of Shapiro and Willoughby (1982):

$$v(r) = V_{max} v'(r/R_{max}). \quad \text{(A1)}$$

At a given multiple or fraction of the radius of maximum wind, the ratio of the local wind to the maximum wind would always be the same. The Rankine vortex, modified Rankine, and Shloemer wind profiles are well represented by (A1), as would be the Holland profile if B had a fixed value. A counterexample is the Holland profile where B changes as a function of V_{max} or R_{max} or simply from one storm to another. The isobaric height in gradient balance with the flow in (A1) is given by

$$g\frac{\partial z}{\partial r} = \frac{v^2}{r} + fv. \quad \text{(A2)}$$

Integration from the vortex center to large radius yields the height–wind relation:

$$g(Z_e - Z_c) = V_{max}^2 \int_0^\infty \frac{v'^2(r/R_{max})}{r}\, dr + fV_{max} \int_0^\infty v'(r/R_{max})\, dr, \quad \text{(A3)}$$

which may be rewritten,

$$g(Z_e - Z_c) = V_{\max}^2 \left[\int_0^\infty \frac{v'^2(r/R_{\max})}{(r/R_{\max})}\, d(r/R_{\max}) + \frac{1}{\mathrm{Ro}} \int_0^\infty v'(r/R_{\max})\, d(r/R_{\max}) \right], \quad \text{(A4)}$$

where $\mathrm{Ro} = V_{\max}/fR_{\max} \cong 10–10^2$ is the Rossby number at the radius of maximum wind. Since the definite integrands contain only $r/R_{\max}$, they would always have the same value if $v'(r/R_{\max})$ always had the same shape. The coefficient of the second term is the only quantity in (A4) that changes with cyclone size or latitude. Thus, apart from a small term proportional to the inverse Rossby number in the eyewall, it is the systematic flattening of the shape function $v'(r/R_{\max})$ with decreasing $V_{\max}$ and increasing $R_{\max}$ and latitude, not the size of the vortex, that controls the proportion between the maximum wind and the geopotential height fall.

REFERENCES

Atkinson, G. D., and C. R. Holliday, 1977: Tropical cyclone minimum sea-level pressure/maximum sustained wind relationship for the western North Pacific. *Mon. Wea. Rev.,* **105,** 421–427.

Black, M. L., J. F. Gamache, F. D. Marks Jr., C. E. Samsury, and H. E. Willoughby, 2002: Eastern Pacific Hurricanes Jimena of 1991 and Olivia of 1994: The effect of vertical shear on structure and intensity. *Mon. Wea. Rev.,* **130,** 2291–2312.

Burpee, R. W., and Coauthors, 1994: Real-time guidance provided by NOAA's Hurricane Research Division to forecasters during Emily of 1993. *Bull. Amer. Meteor. Soc.,* **75,** 1765–1783.

Callaghan, J., and R. K. Smith, 1998: The relationship between maximum surface wind speeds and the central pressure in tropical cyclones. *J. Aust. Meteor. Soc.,* **47,** 191–202.

Franklin, J. L., M. L. Black, and K. Valde, 2003: GPS dropwindsonde wind profiles in hurricanes and their operational implications. *Wea Forecasting,* **18,** 32–44.

Gray, W. M., 1984: Atlantic seasonal hurricane frequency. Part I: EI Niño and 30 mb quasi-biennial oscillation influences. *Mon. Wea. Rev.,* **112,** 1649–1668.

——, and D. J. Shea, 1973: The Hurricane's inner core region. II. Thermal stability and dynamic characteristics *J. Atmos. Sci.,* **30,** 1565–1576.

Ho, F. P., J. C. Su, K. L. Hanevich, R. J. Smith, and F. P. Richards, 1987: Hurricane climatology for the Atlantic and Gulf Coasts of the United States. NOAA Tech. Memo. NWS-38, National Weather Service, Silver Spring, MD, 195 pp.

Holland, G. J., 1980: An analytic model of the wind and pressure profiles in hurricanes. *Mon. Wea. Rev.,* **108,** 1212–1218.

Jarvinen, B. R., and M. B. Lawrence, 1985: An evaluation of the SLOSH storm-surge model. *Bull. Amer. Meteor. Soc.,* **66,** 1408–1411.

——, C. J. Neumann, and M. A. S. Davis, 1984: A tropical cyclone data type for the North Atlantic Basin, 1886–1983: Contents, limitations, and uses. NOAA Tech. Memo. NWS NHC 22, Coral Gables, FL, 21 pp.

Jelesnianski, C. P., 1967: Numerical computation of storm surges with bottom stress. *Mon. Wea Rev.,* **95,** 740–756.

Jordan, C. L., 1958: Mean soundings for the West Indies area. *J. Meteor.,* **15,** 91–97.

Jorgensen, D. P., 1984a: Mesoscale and convective-scale characteristics of mature hurricanes. Part I: General observations by research aircraft. *J. Atmos. Sci.,* **41,** 1268–1285.

——, 1984b: Mesoscale and convective-scale characteristics of mature hurricanes. Part II: Inner core structure of Hurricane Allen (1980). *J. Atmos. Sci.,* **41,** 1287–1311.

Myers, V. A., 1957: Maximum hurricane winds. *Bull. Amer. Meteor. Soc.,* **38,** 227–228.

Neumann, C. J., B. R. Jarvinen, C. J. McAdie, and G. R. Hammer, 1999: *Tropical Cyclones of the North Atlantic Ocean, 1871–1998.* Historical Climatology Series, Vol. 6-2, NOAA, 206 pp.

Pielke, R. A., Jr., and C. W. Landsea, 1998: Normalized hurricane damages in the United States: 1925–95. *Wea. Forecasting,* **13,** 621–631.

——, J. Rubiera, C. Landsea, M. L. Fernandez, and R. Klein, 2003: Hurricane vulnerability in Latin America and the Caribbean: Normalized damage and loss potentials. *Nat. Hazards Rev.,* **4,** 101–114.

Press, W. H., B. P. Flannery, S. A. Teukolsky, and W. T. Vettering, 1986: 10.1 Golden section search in one dimension. *Numerical Recipes: The Art of Scientific Computing,* Cambridge University Press, 277–282.

Rappaport, E. N., 2000: Loss of life in the United States associated with recent Atlantic tropical cyclones. *Bull. Amer. Meteor. Soc.,* **81,** 2065–2074.

Riehl, H., 1963: Some relationships between wind and thermal structure of steady state hurricanes. *J. Atmos. Sci.,* **20,** 276–287.

Schloemer, R. W., 1954: Analysis and synthesis of hurricane winds over Lake Okechobee, Florida. Hydrometeorological Rep. 31, U.S. Weather Bureau, Department of Commerce, and Army Corps of Engineers, 39 pp.

Schubert, W. H., and J. J. Hack, 1982: Inertial stability and tropical cyclone development. *J. Atmos. Sci.,* **39,** 1687–1697.

Shapiro, L. J., and H. E. Willoughby, 1982: The response of balanced hurricanes to local sources of heat and momentum. *J. Atmos. Sci.,* **39,** 378–394.

Shea, D. J., and W. M. Gray, 1973: The hurricane's inner core region. I. Symmetric and asymmetric structure. *J. Atmos. Sci.,* **30,** 1544–1564.

Sheets, R. C., 1969: Some mean hurricane soundings. *J. Appl. Meteor.,* **8,** 134–146.

Smith, R. K., 1981: The cyclostrophic adjustment of vortices with application to tropical cyclone modification. *J. Atmos. Sci.* **38,** 2021–2030.

Thompson, E. F., and V. J. Cardone, 1996: Practical modeling of hurricane surface wind fields. *J. Waterw. Port Coastal Ocean Eng.,* **122,** 195–205.

Vickery, P. J., and L. A. Twisdale, 1995: Prediction of hurricane wind speeds in the United States. *J. Struct. Eng.,* **121,** 1691–1699.

Willoughby, H. E., 1990a: Temporal changes of the primary circulation in tropical cyclones. *J. Atmos. Sci.,* **47,** 242–264.

——, 1990b: Gradient balance in tropical cyclones. *J. Atmos. Sci.,* **47,** 265–274.

——, and M. B. Chelmow, 1982: Objective determination of hurricane tracks from aircraft observations. *Mon. Wea. Rev.,* **110,** 1298–1305.

——, J. A. Clos, and M. B. Shoreibah, 1982: Concentric eyewalls, secondary wind maxima, and the evolution of the hurricane vortex. *J. Atmos. Sci.,* **39,** 395–411.

——, D. P. Jorgensen, R. A. Black, and S. L. Rosenthal, 1985: Project STORMFURY: A scientific chronicle 1962–1983. *Bull. Amer. Meteor. Soc.,* **66,** 505–514.